INTERNATIONAL JOURNAL OF RESEARCH IN AERONAUTICAL AND MECHANICAL ENGINEERING

ISSN (ONLINE): 2321-3051

Vol.2 Issue.12,

December 2014.

Pgs: 11-23

Vibration Analysis of Dragonfly wing section in Gliding Mode at Low Reynolds Numbers

Husain Mehdi[1], Sayed Fahad Anwer[2], Akhlaque Ahmad[2]

[1]Assitant Professor, MED, Meerut Institute of Technology, Meerut (U.P), 250002/ INDIA

[2]Department of Mechanical Engineering ZHCET, AMU Aligarh, 202002/ INDIA

Abstract

The dragonfly wings are highly corrugated, due to light in weight and good corrugation it increases the aerodynamic performance and strength of the wing. When the wings interact with the air, it is subjected to aerodynamic forces acting on the surface of the wing and the inertial force due to the acceleration or deceleration of the wing mass. The interaction between these inertial and aerodynamic forces resulted in wing deformation. We are interesting to calculate deformation and natural frequency of the dragon fly wing at different Reynolds number and different angle of attack. A dragonfly insect has been chosen because MAVs (Micro air Vehicles) and Dragonfly works almost same Reynolds Number i.e. Re- 10^2 to 10^4. In this work, Numerical study of Vibration Analysis for a Pleated Insect 2D Airfoil at Ultra Low Reynolds Numbers is carried out in gliding mode. The dynamics of a pleated insect wing subjected to aerodynamic loading is studied for different Reynolds Number ranging from 100 to 1000 at different angle of attack ranging from 0^0 to 15^0 by using ANSYS-14 multi physics solver. The result from the CFD solver will be fed in the form of lift and drag forces are then fed into the ANSYS Workbench solver and vibration analysis is performed.

Keywords: Lift Coefficient, Drag Coefficient. Angle of Attack, Reynolds No, Deflection, Natural Frequency.

1 Introduction

Aeshna genus dragon fly can glide up to 30s without any significant loss of altitude [1]. A smaller dragon flies found there gliding periods lasting 0.5s, covering a distance of approximately 1m and thus achieving gliding speed of $2.5ms^{-1}$. Thus the typical range of Reynolds number in gliding flight can vary from 10^2 [2]. compared aerodynamic performance of cross-sections at different positions along the span of a wing of an Aeschna cyanea to develop the pleated models and its corresponding profiled airfoil at a chord Reynolds number of 10 000, and the results showed that the pleated airfoils generated higher lift than the profiled airfoils [3]. The orientation of the leading edge does not have an effect in enhancing the lift production [3] [4]. As with the early flow visualization experiments, trapped vortices present in the folds that serve to change the effective profile of the airfoil [3]. Dragon flies have corrugated wings where the pleated configuration varies along the span-wise and chord-wise and also studied the aerodynamic performance of a pleated wing section based on the wing of Aeshna cyanea has been performed at ultra-low Reynolds numbers (5000-10000) corresponding to the gliding flight of these dragonflies in two dimension using computational fluid dynamics. The simulations demonstrate that the pleated airfoil produces comparable and at times higher lift than the profiled airfoil, with a drag comparable to that of its profiled counterpart [5]. The effect of the Reynolds number on the gliding ratio is that at Re 1000 and at angle of attack

(here after, AOA) 15^0, the largest gliding ratios are obtained. Flow invariably for all Reynolds number, minimum Drag coefficient is obtained at AOA 15^0 [6].

Micro air vehicles (MAVs offer great potentials for various civil and military applications in revolutionizing sensing and information gathering, such as surveillance, inspection, targeting, or biochemical sensing tasks at remote and hazardous locations. Numerous vehicle concepts, including fixed, rotary, and flapping wings, have been proposed [7][8]. However, the advantage of a flapping wing in MAV compared with fixed or rotary-wing aircraft of the same scale is emphasized by its maneuverability and smooth transition from hovering to forward flight signature [9][10].

The structural deformation during flapping can significantly influence the flow behavior around the wing and, consequently, brings an important on its aerodynamic performance [11]. Physiological studies have shown that insect wing deformation is passive in which the wing is deformed by both inertial acceleration and deceleration of the wing mass, by the aerodynamic force from surrounding air, or by the combination of both [12]. The overall bending patterns of a hawkmoth wing are quite similar when flapped (single degree-of-freedom flap rotation) in air and in helium, despite an 85% reduction in fluid density [11]. The wing deformation leads to substantial power economy for lift production. Moreover, they noticed that the leading-edge vortex (LEV) in the full- kinematic model remains attached to the wing during the entire flapping cycle, which may have contributed to the aerodynamic power efficiency of the wing [13]. The quantitative data on the time-varying camber and twist of the wing in free-flying drone flies [14]. A further study was conducted where they removed the camber and spanwise twist one by one and they observed that the lift in the free-flying drone flies is principally caused by camber deformation [15].

In this work, we investigate Modal Analysis for spatio-temporal dynamics of a cut section of Aeshna Cyanea's wing at ultra low Reynolds numbers (100 to 1000) at different angle of attacks ranging from 0^o to 15^o. To the best of author's knowledge, The Modal Analysis of 2D pleated airfoil is not studied. These parameter ranges are relevant for both dragon flies and micro-aerial vehicles. Past experimental studies have found no intrinsic three-dimensional effects at these low Reynolds numbers. Thus, 2D simulations are implemented in this study to encompass a relatively wide range of the parameter space necessary to draw some general conclusions regarding pleated airfoils. The pleated airfoil implemented in the numerical simulation corresponds to a cross-section located at the mid-section of the forewing of a dragonfly (Aeshna cyanea) [3][4]. The specific profile chosen for the numerical simulations corresponds to 'Profile 2', which was digitally extracted from the paper [3][5]. From the three pleated geometries to select from the paper of [3], 'Profile 2' was chosen due to its horizontal leading edge, thus eliminating the issue that the orientation of the leading edge has an influence on the aerodynamic performance [4]. For the purposes of reducing the resolution requirements in the simulation, the sharp edges of the pleats were rounded out slightly without affecting the basic geometry of the pleats and the overall shape of the airfoil as shown in Figure-2. The shape-forming and stiffness-adjusting mechanisms of a cell through its inner filled liquid have inspired some air-supported/liquid-supported inflatable structural systems [16] [17].

(a)Profile 1 (b) Profile 2 (c) Profile 3

Figure 1: An Illustration of different cut section profiles used by Kessel (2006) and Vargas et al (2008)

INTERNATIONAL JOURNAL OF RESEARCH IN AERONAUTICAL AND MECHANICAL ENGINEERING

ISSN (ONLINE): 2321-3051

Vol.2 Issue.12,

December 2014.

Pgs: 11-23

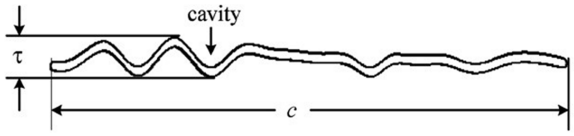

Figure 2: The two-dimensional airfoils used in the numerical simulation. Pleated airfoil representing a cross-section of the forewing of a dragonfly (Aeshna cyanea) having τ /c = 7.531%

2 Governing Equation

2.1 Fluid Flow

The equations governing the flow in the numerical solver are the time-dependent, viscous incompressible Navier–Stokes equations. The non-dimensional momentum and continuity equations are as follows:

$$\frac{\partial u_i}{\partial x_i} = 0 \quad (1)$$

$$\frac{\partial u_i}{\partial t} + \frac{\partial u_i u_j}{\partial x_j} = -\frac{\partial p}{\partial x_i} + \frac{1}{Re}\frac{\partial^2 u_i}{\partial x_j \partial x_j} \quad (2)$$

The equations are non-dimensionalized with the appropriate length and velocity scales, in this case the airfoil chord and free stream velocity. Here Re corresponds to the Reynolds number which is defined as below:

$$Re = \frac{\rho u_\infty c}{\mu} \quad (3)$$

Using the same flow parameters and geometrical dimensions as Kesel (2000), this allowed for validation and a critical analysis of the numerical results. The key quantities examined are the lift and drag coefficients which are defined as

$$C_L = \frac{F_L}{\frac{1}{2}\rho u_\infty^2 c}, \quad (4)$$

$$C_D = \frac{F_D}{\frac{1}{2}\rho u_\infty^2 c} \quad (5)$$

$$\text{Gliding Ratio} = \frac{C_L}{C_D} \quad (6)$$

2.2 Structure Analysis:

The interaction of the fluid and the structure at a mesh interface causes the acoustic pressure to exert a force applied to the structure and the structural motions produce an effective "fluid load." The governing finite element matrix equations then become

$$[M_S]\{\ddot{U}\} + [K_S]\{U\} = \{F_S\} + [R]\{P\} \quad (7)$$

$$[M_f]\{\ddot{P}\} + [K_f]\{P\} = \{F_f\} - \rho o\,[R]^T\{\ddot{U}\} \quad (8)$$

[R] is a "coupling" matrix that represents the effective surface area associated with each node on the fluid-structure interface (FSI). The coupling matrix [R] also takes into account the direction of the normal vector defined for each pair of coincident fluid and structural element faces that comprises the interface surface. The positive direction of the normal vector, as the program uses it, is defined to be outward from the fluid mesh and in towards the structure. Both the structural and fluid load quantities that are produced at the fluid-structure interface are functions of

unknown nodal degrees of freedom. Placing these unknown "load" quantities on the left hand side of the equations and combining the two equations into a single equation produces the following.

2.3 Modal Analysis

2.3.1 *Damping Matrices*

Damping may be introduced into a transient, harmonic, or damped modal analysis as well as a response spectrum. The type of damping allowed depends on the analysis as described in the subsequent sections.

2.3.2 *Transient Analysis and Damped Modal Analysis*

The damping matrix, [C], may be used in transient and damped modal analyses as well as substructure generation. In its most general form, the damping matrix is composed of the following components.

$$[C]=\alpha[M]+(\beta+\frac{2}{\Omega}g)[K]+\sum_{i=1}^{N_{ma}}\alpha_i^{m}[M_i]+\sum_{j=1}^{N_m}[(\beta_j^{m}+\frac{2}{\Omega}g_j+\frac{1}{\Omega}g_j^{E})[K_j]]+\sum_{k=1}^{N_e}[C_k]+\sum_{m=1}^{N_v}\frac{1}{\Omega}[C_m]+\sum_{l=1}^{N_g}[G_l] \quad (9)$$

where: [C] = structure damping matrix, α = mass matrix multiplier, [M] = structure mass matrix, β = stiffness matrix multiplier, [K] = structure stiffness matrix, N_{ma} = number of materials, α_i^{m} = mass matrix multiplier for material i, $[M_i]$ = portion of structure mass matrix based on material i, N_{mb} = number of materials, $[K_j]$ = portion of structure stiffness matrix based on material j, N_e = number of elements with specified damping, $[C_k]$ = element damping matrix, Ng = number of elements with Coriolis or gyroscopic damping, $[G_l]$ = element Coriolis or gyroscopic damping matrix, β_j^{m} = stiffness matrix multiplier for material.

2.3.3 *Harmonic Analysis*

The damping matrix ([C]) used in harmonic analyses is composed of the following components.

$$[C]=\alpha[M]+(\beta+\frac{2}{\Omega}g)[K]+\sum_{i=1}^{N_{ma}}\alpha_i^{m}[M_i]+\sum_{j=1}^{N_m}[(\beta_j^{m}+\frac{2}{\Omega}g_j+\frac{1}{\Omega}g_j^{E})[K_j]]+\sum_{k=1}^{N_e}[C_k]+\sum_{m=1}^{N_v}\frac{1}{\Omega}[C_m]+\sum_{l=1}^{N_g}[G_l] \quad (10)$$

The input exciting frequency, Ω, is defined in the range between Ω_B and Ω_E via

$\Omega_B = 2\pi f_B$, $\Omega_E = 2\pi f_E$, f_B = beginning frequency, f_E = end frequency

Substituting equation (10) into the harmonic response equation of motion and rearranging terms yields

$$[[K]+i\{2g[K]+\sum(2g_j+g_j^{E})[K_j]+\sum[C_m]\}+i\Omega[\alpha[M]+\sum\alpha_i^{m}[M_i]+\beta[K]+\sum\beta_j^{m}[K_j]+\sum[C_k]+\sum[G_j]]](u_1+iu_2)=F_1-\Omega^2[M] \quad (11)$$

The complex stiffness matrix in the first row of the equation consists of the normal stiffness matrix augmented by the structural damping terms given by g, g_i, g_i^E, and $[C_m]$ which produce an imaginary contribution. Structural damping is independent of the forcing frequency, Ω, and produces a damping force proportional to displacement (or strain). The terms g, g_i, and g_i^E are damping ratios (i.e., the ratio between actual damping and critical damping, not to be confused with modal damping).
The second row consists of the usual viscous damping terms and is linearly dependent on the forcing frequency, Ω, and produces forces proportional to velocity.

2.3.4 *Mode-Superposition Analysis*

The damping matrix is not explicitly computed, but rather the damping is defined directly in terms of a damping ratio ξd. The damping ratio is the ratio between actual damping and critical damping. The damping ratio ζ_i^d for mode i is the combination of

$$\zeta_i^d = \zeta + \zeta_i^m + \frac{\alpha}{2\omega_i} + \frac{\beta}{2}\omega_i \tag{12}$$

ξ = constant modal damping ratio, ζ_i^m = modal damping ratio for mode shape i (see below), ω_i = circular natural frequency associated with mode shape i = $2\pi f_i$, f_i = natural frequency associated with mode shape i, α = mass matrix multiplier

The modal damping ratio ζ_i^m can be defined for each mode directly (undamped modal analyses only).

Alternatively, for the case where multiple materials are present whose damping ratios are different, an effective mode-dependent damping ratio ζ_i^m can be defined in the modal analysis if material-dependent damping is defined and the element results are calculated. This effective damping ratio is computed from the ratio of the strain energy in each material in each mode using,

$$\zeta_i^m = \frac{\sum_{j=1}^{N_m} \beta^m{}_j E_j^s}{\sum_{j=1}^{N_m} E_j^s} \tag{13}$$

3 Numerical Methodology

Ansys Fluent 14.0 is used to solve the above equations. The solver used is based on collocated methodology and finite volume discretization technique is used.

$$\iiint \frac{\partial \rho \emptyset}{\partial t} dV + \oint \rho \emptyset \vec{v} . d\vec{A} = \oint \Gamma_\phi \nabla \emptyset . d\vec{A} + \iiint S_\emptyset \, dV \tag{14}$$

$$\frac{\partial \rho \emptyset}{\partial t} V + \sum_{f}^{N_{faces}} \rho_f \vec{v}_f \phi_f . \vec{A}_f = \sum_{f}^{N_{faces}} \Gamma_\phi \nabla \phi_f . \vec{A}_f + S_\phi V$$

The gradients are calculated using Green-Gauss Cell-Based methodology proposed by [21] [22].

$$\overline{\emptyset_f} = \frac{1}{N_f} \sum_{n}^{N_f} \overline{\emptyset}_n \quad (15)$$

where N_f is the number of nodes on the face Convection terms in the momentum equation are discretized using the second order upwind methodology given by in the second order up wind quantities at cell faces are computed using a multidimensional linear reconstruction approach [23]. The result from the CFD solver will be fed in the form of lift and drag forces are then fed into the ANSYS Workbench solver and one way Fluid Structure Interaction analysis is performed.

4 Grid Design:

The pleated cross section of modeled dragon fly is taken from the paper [5]. The length of pleated plate is assumed to be of unit length by giving X coordinate=1, Height is also given to pleated section in the Y direction and it is 0.05. The pleated section is covered with a circular region of diameter 20C where C is set to 1.This circular region is then divided into 2 parts along semi-circle parallel to Y axis.Then 150 nodes are taken on each semi circle.60 nodes are also taken on airfoil's upper and lower part.Then command of triangular meshing is giving and the required meshed profile is obtained.

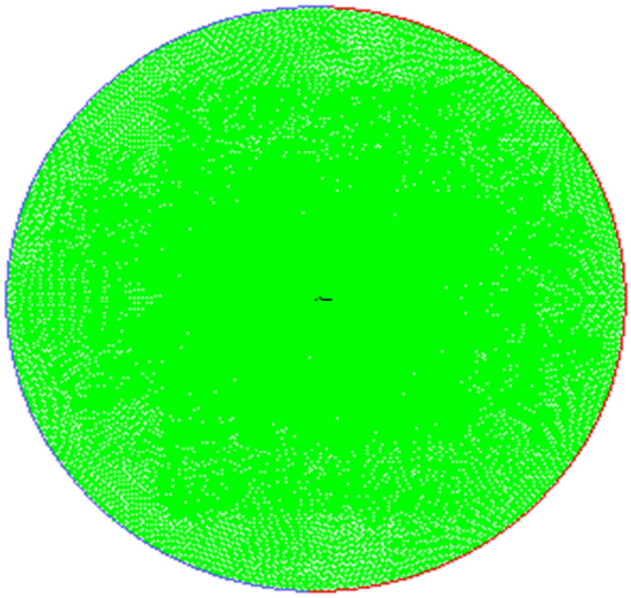

Figure 3:- Mesh of the problem

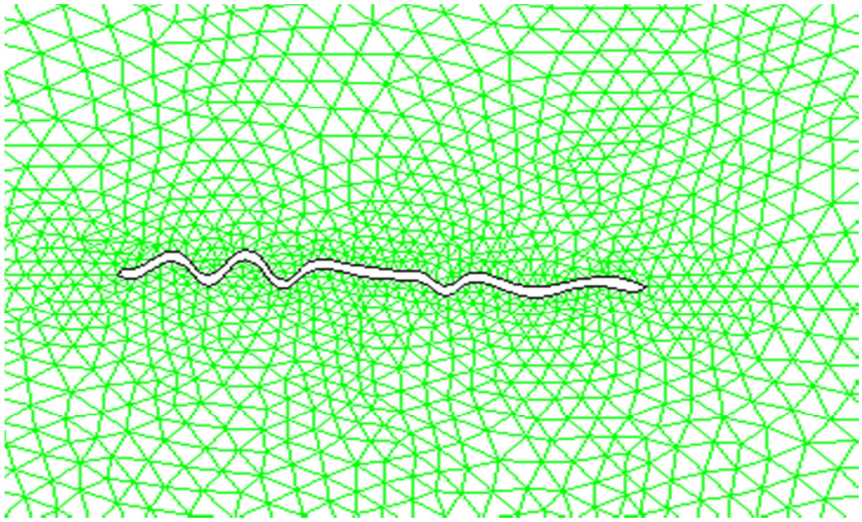

Figure 4:- The zoomed view of the mesh

Grid information:

- 195834 triangular cells
- 196878 nodes,
- Inflow and out flow boundaries are pressure far field
- Inner meshed region is fluid.

Face area statistics:

- Minimum face area (m^2) : 4.428917 e-003
- Maximum face area (m^2) : 2.160249 e-001

5 Boundary Condition

A constant velocity u= 0.14607 m/sec is imposed on the left side of grid, and the right side set as an outflow region where the gradient values are set to zero. The components are taken in accordance with the angle of attack. Pressure on the both sides was taken as atmospheric i.e. $P=P_{atm}$

Velocity inlet boundary conditions are used to define the velocity and scalar properties of the flow at inlet boundaries.

Out flow boundary condition are used to model flow exits where the details of the flow velocity and pressure are not known prior to solution of the flow problem. They are appropriate where the exit flow is close to a fully developed condition, as the out flow boundary condition assumes a zero normal gradient for all flow variables except pressure.

6 Results and Discussions

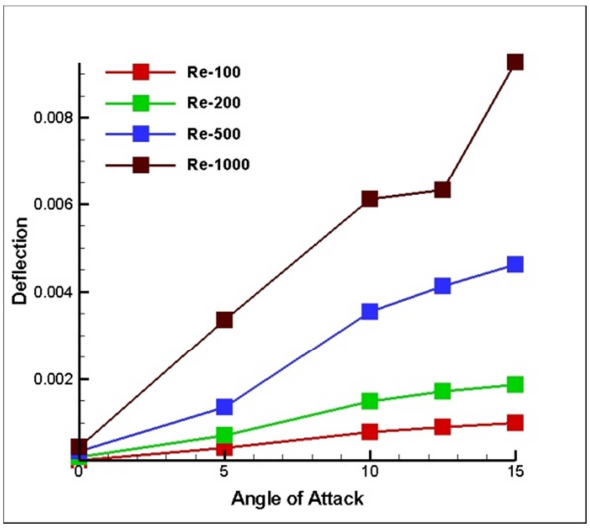

(a)

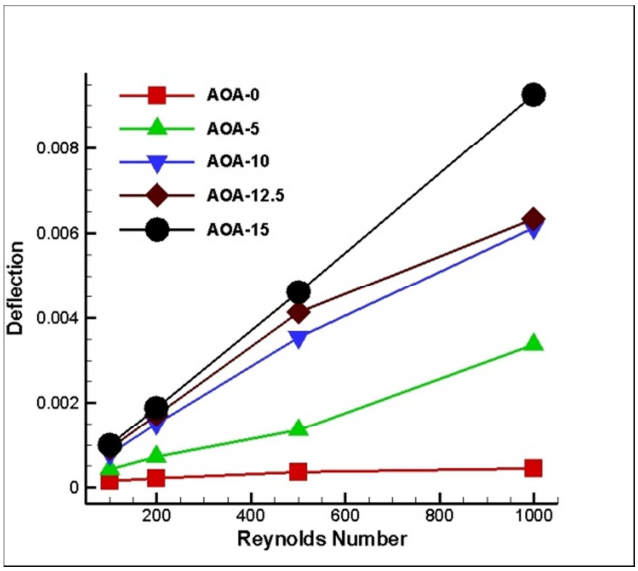

(b)

Figure-5:- (a) Variation of deflection and AOA, (b) Variation of deflection and Re

The material density of wing ρ is taken as 1,200 kg/ [18], and confirmed by Vincent and Wegst [19] and we used a Poisson's ratio ν of 0.49 [18]. Combes and Daniel [11] also used a Poisson's ratio of 0.49.

ANSYS 14 was utilized to solve this model of a dragonfly wing, and airfoil was assumed to be fully clamped along the wing root. Figure-5 shows the variation of deflection and angle of attack. It is seen to be that deflection is increased with increasing the Reynolds Number with their angle of attack. The maximum deflection occur in Re-1000, angle of attack 15^0 i.e. 9.2597x1 0^{-3} mm and minimum value of deflection occurs in Re-100 with angle of attack 0^0 i.e.1.4618 x 10^{-4} mm. we have calculated all six modes of vibration, according to figure-6 the minimum value of natural frequency is 0.6985 and the maximum natural frequency is 34.353 Hz which are bending and torsional mode respectively.

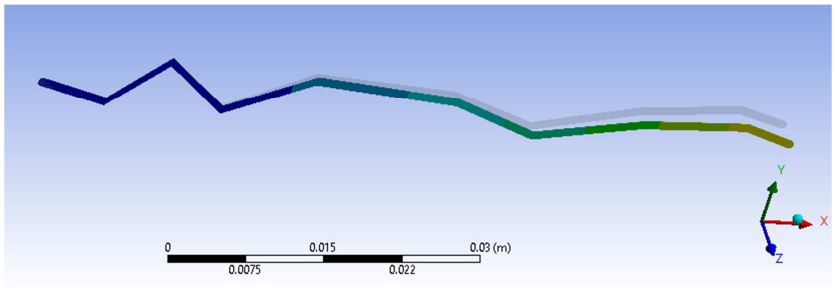

(a)

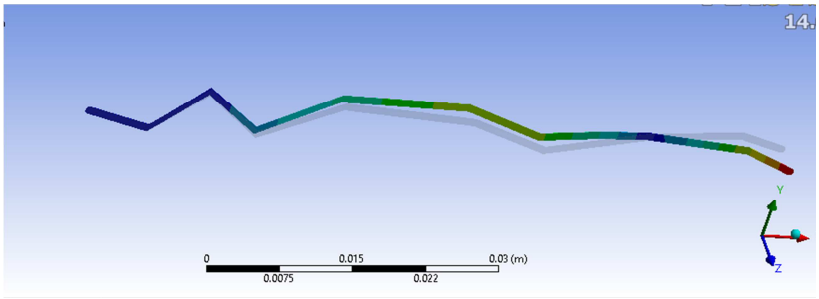

(b)

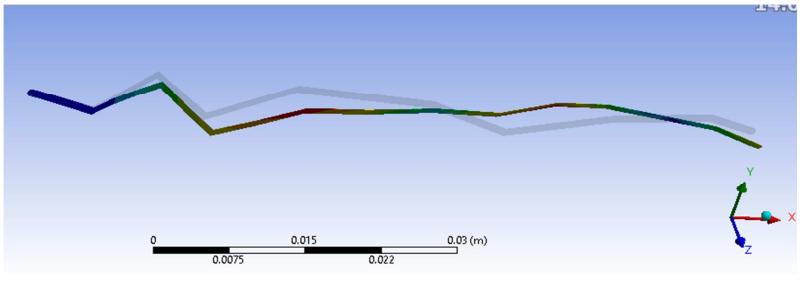

(c)

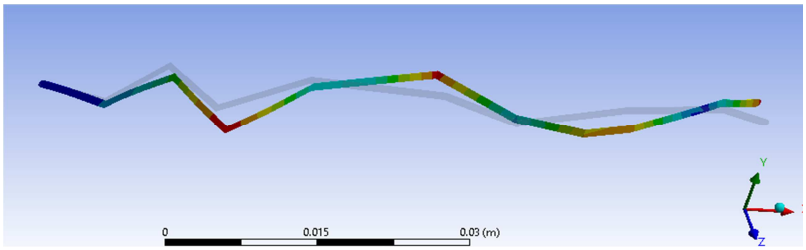

(d)

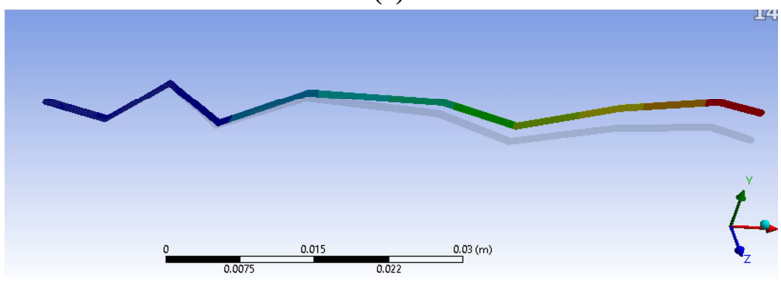

(e)

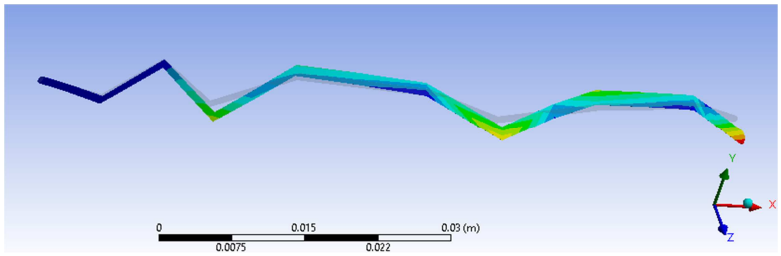

(f)

Figure 6:- (a) Mode Shape 1 at 0.69851Hz,(b) Mode Shape 2 at 4.439 Hz,(c) Mode Shape 3 at 12.523 Hz, (d) Mode Shape 4 at 21.259 Hz,(e) Mode Shape 5 at 23.561 Hz,(f) Mode Shape 6 at 34.353 Hz

Table 1:- Validation

Wing Model	Mode Shape	Natural frequency	Type	Authors
2D	1^{st}	32.30 Hz	Bending	Wootton [12]
	5^{th}	23.56 Hz	Bending	Present
	1^{st}	25.40 Hz	Bending	Jongerius [20]

In this work, results of free vibration analysed. In which we neglect damping, show the same deformation for the natural modes as Wootton [12] found bending for the first natural mode and torsion for the second natural mode. In our two dimensional model the fifth natural frequency 23.561 Hz is close to the flapping frequency 32.3 Hz (Table 1).

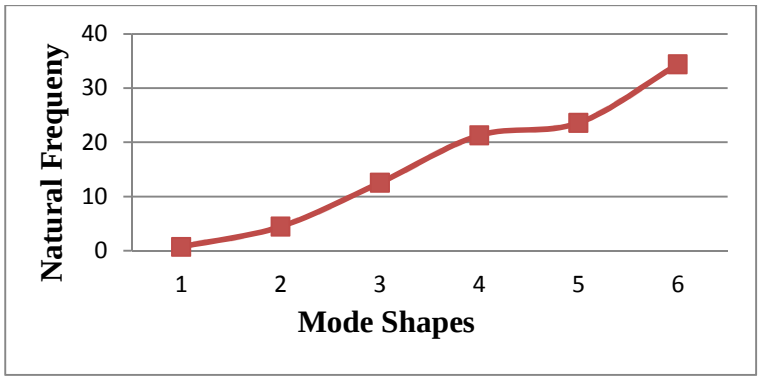

Figure 7:- Variation of Natural Frequency and Mode Shapes

7 Conclusions

In this work we find the natural frequency of dragonfly's wing in different modes. The strategy of dragonflies to flap their wings at a much lower frequency than the natural vibration frequency of their forewing is contrasted by the most advanced flapping wings designed for micro air vehicles [20]. We investigated Modal Analysis for spatio-temporal dynamics of a cut section of Aeshna Cyanea's wing. Numerical simulations were performed at ultra low Reynolds numbers (100 to 1000) at different angle of attacks ranging from 0^0 to 15^0. The results give a satisfactory measure of confidence in the fidelity of the simulation. The deflection is increased when we increased the Reynolds Number with increase their angle of attack The maximum deflection occur in Re-1000, angle of attack 15^0 i.e. 9.2597×10^{-3} mm and minimum value of deflection occurs in Re-100 with angle of attack 0^0 i.e.1.4618×10^{-4} mm..the highest natural frequency 34.353 Hz was found in mode 6 which is torsional mode, whereas minimum natural frequency 0.6951 was found in mode 1.

References:

[1] Brodsky, A K. The aerodynamics of insect flight: The Evolution of Insect flight. New York: Oxford University Press, 1994.

[2] Wakeling JM,EllingtonCP, "Dragonfly flight: III. Lift and power requirements". *The Journal of Experimental Biology* 200:583–600, 1997.

[3] Kesel, A B. "Aerodynamic characteristics of dragonfly wing sections compared with technical aerofoil." J of Exp. Biology 203 (2000): 3125-3135.

[4] Okamoto, M, K Yasuda, and A Azuma. "Aerodynamic characteristics of the wings and body of a dragonfly." J. of Experimental Biology, 1996: 281-294.

[5] Vargas, Abel, Rajat Mittal, and Haibo Dong. "A computational study of the aerodynamic performance of a dragonfly wing section in gliding flight." Bioinsp. Biomim., 2008: 1-13.

[6] Anwer SF, Ashraf I, Mehdi H, (2013) "On the Aerodynamic Performance of Dragonfly Wing Section in Gliding Mode" Advances in Aerospace Science and Applications. Vol 3, pp 227-234.

[7] Shyy W, Berg M, Ljungqvist D, " Flapping and flexible wings for biological and micro air vehicles". *Progress in Aerospace Sciences* 35(5):455–505, 1999.

[8] Mueller TJ, " Fixed and flapping wing aerodynamics for micro air vehicle applications", *Progress in Astronautics and Aeronautics* 195, 2001.

[9] Lian YS, Shyy W, Viieru D, Zhang B (2003). Membrane wing aerodynamics for micro air vehicles. *Progress in Aerospace Sciences* 39:425–465

[10] Ramasamy M, Leishman JG, Lee TE (2006). Flow field of a rotating wing MAV. *Proceedings of 62nd Annual National Forum of the American Helicopter Society*. May 9-11 2006.

[11] Combes SA, Daniel TL, "Into thin air: contributions of aerodynamic and inertial-elastic forces to wing bending in the hawkmothManducasexta". *The Journal of Experimental Biology* 206:2999–3006, 2003.

[12] Wootton RJ, Herbert RC, Young PG, Evans KE, " Approaches to the structural modelling of insect wings". *Philosophy Transaction Royal Society* 358(1437):1577-1587, 2003.

[13] Young SM, Walker RJ, Bomphrey GK, Taylor, Thomas ALR, " Details of insect wing design and deformation enhance aerodynamic function and flight efficiency", *Science* 325(5947):1549-1552, 2009.

[14] Walker J, Thomas ALR, Taylor GK, " Deformable wing kinematics in free-flying hoverflies", *Journal of Royal Society Interface* 7(42):131-142, 2010.

[15] Du G, Sun M (2010), " Effects of wing deformation on aerodynamic forces in hovering hoverflies", *The Journal of Experimental Biology* 213:2273-2283, 2010.

[16] Schlaich, J., Bergermann, R., Sobek, W, "Air-inflated roof over the Roman amphitheatre at Nimes". *Structural Engineering Review*, **6**(3-4):203-214, 1994.

[17] Bradshaw, R., Campbell, D., Gargari, M., Mirmiran, A.,Tripeny, P., 2002. Special structures: past, present, and future. *Journal of Structural Engineering ASCE*, **128**(6):691-709

[18] Wainwright SA, Biggs WD, Currey JD and Gosline JM ,"Mechanical design in organisms", Princeton University Press, 1982.

[19] Vincent JFV, Wegst UGK, "Design and mechanical properties of insect cuticle", Arthropod Stru Dev 33:187–199, 2004.

[20] Lentink D, Jongerius SR and Bradshaw NL, "The scalable design of flapping micro air vehicles inspired by insect flight, 2009.

[21] Holmes D.G. and Connell S.D., "Solution of the 2D Navier-Stokes Equations on Unstructured Adaptive Grids", Presented at the AIAA 9th Computational Fluid Dynamics Conference, June, 1989.

[22] Rauch R.D., Batira, J.T. and Yang N.T.Y., "Spatial Adaption Procedures on Unstructured Meshes for Accurate Unsteady Aerodynamic Flow Computations ",Technical Report AIAA-91-1106, AIAA, 1991.

[23] Barth T.J. and Jespersen D., "The design and application of upwind schemes on unstructured meshes", Technical Report AIAA-89-0366, AIAA 27th Aerospace Sciences Meeting, Reno, Nevada, 1989.

*Corresponding Author, Husain Mehdi have done his M.Tech (Machine Design) from **Aligarh Muslim University, Aligarh, (U.P), India**. Now he is an Assistant Professor in the Department of Mechanical Engineering towards the growth of professionally managed organization Meerut Institute of Technology, Meerut, past 3 years. His core area of interest is Machine design, and is continuously performing research work on computational fluid Dynamics, Composite Material, Material Science and many more.